nature genetics

Secretory COPII coat component Sec23a is essential for craniofacial chondrocyte maturation

Michael R Lang[1–3,7], Lynne A Lapierre[4], Michael Frotscher[5], James R Goldenring[2,4,6] & Ela W Knapik[1–3]

An increasing number of human disorders have been linked to mutations in genes of the secretory pathway. The chemically induced zebrafish *crusher* variant results in malformed craniofacial skeleton, kinked pectoral fins and a short body length. By positional cloning, we identified a nonsense mutation converting leucine to a stop codon (L402X) in the *sec23a* gene, an integral component of the COPII complex, which is critical for anterograde protein trafficking between endoplasmic reticulum and Golgi apparatus. Zebrafish *crusher* mutants develop normally until the onset of craniofacial chondrogenesis. *crusher* chondrocytes accumulate proteins in a distended endoplasmic reticulum, resulting in severe reduction of cartilage extracellular matrix (ECM) deposits, including type II collagen. We demonstrate that the paralogous gene *sec23b* is also an essential component of the ECM secretory pathway in chondrocytes. In contrast, knockdown of the COPI complex does not hinder craniofacial morphogenesis. As *SEC23A* lesions cause the cranio-lenticulo-sutural dysplasia syndrome, *crusher* provides the first vertebrate model system that links the biology of endoplasmic reticulum to Golgi trafficking with a clinically relevant dysmorphology.

Secretion is an elemental function of every cell. Elegant studies have identified many of the molecular steps in the anterograde protein trafficking from the endoplasmic reticulum to the Golgi apparatus. However, most experiments have been conducted *in vitro* with purified components or *in vivo* using unicellular yeast or mammalian cells in culture as model systems. Less is known about the behavior of the secretory pathway within the context of the entire multicellular organism and how its malfunction might influence development and organ homeostasis.

In yeast, COPII-coated vesicles provide the primary means of cargo export[1]. COPII (coat protein II) vesicle formation is initiated by Sec12p recruitment of GDP-bound cytosolic Sar1p to the endoplasmic reticulum membrane. Sec12p-dependent Sar1p-GTP activation is followed by binding of cytoplasmic Sec23p/Sec24p heterodimers to the Sar1p-GTPase[2,3]. Sec24p acts in cargo selection, whereas both Sec23p and Sec24p recruit Sec13p/Sec31p complexes, which create the structural part of the coat[4–6]. Sec31p then promotes coat polymerization and budding of cargo-loaded vesicles *en route* to the Golgi complex.

Typically, 60- to 90-nm COPII coated vesicles are sufficient to transport small globular proteins. In contrast, cartilage development requires efficient production and export of matrix proteins to the extracellular space. Cartilage ECM primarily consists of fibrillar type II collagen that exits from the endoplasmic reticulum as large 300-nm procollagen bundles[7,8]. Studies in mammalian cells showed that large procollagen cargo might be transported to Golgi by a specialized endoplasmic reticulum–Golgi intermediate compartment (ERGIC) also known as vesicular tubular cluster (VTC) complexes in a COPII-dependent manner[9]. Moreover, the COPI complex, primarily responsible for retrograde membrane recycling between Golgi and endoplasmic reticulum, has been implicated in cargo sorting at the level of ERGIC and has been found to colocalize to vesicles moving from ERGIC to Golgi[10,11].

Zebrafish cranial skeleton develops within the first 3 d post-fertilization (dpf) and is primarily built from cartilage elements that later ossify (**Fig. 1** and **Supplementary Fig. 1** online). The zebrafish *crusher* mutation was recovered during a chemical mutagenesis screen for phenotypes affecting craniofacial development[12]. Its primary features are short body length, small and malformed head skeleton and absence of cartilaginous ear capsules (**Fig. 1d**,**f**,**h**). The neurocranium is reduced to approximately 40% of the wild-type length and lacks parachordal cartilages, an integral part of the ear capsule, suggesting failure of isometric cartilage growth. Histological analysis showed accumulation of ECM within developing chondrocytes, indicating a defect in the secretory pathway (**Fig. 1i**,**j**).

To establish the chromosomal localization of the *crusher* mutation, we used linkage analysis in ~2,000 meioses from a F2 intercross using the zebrafish simple sequence length polymorphism (SSLP) genetic map[13]. Based on fine mapping of the *crusher* locus and comparison with human and mouse syntenic regions, we identified *sec23a*, a structural component of the endoplasmic reticulum–derived COPII complex, as a likely candidate gene (**Fig. 2a**). Sequencing of the *sec23a*

[1]Department of Medicine, Division of Genetic Medicine and [2]Department of Cell and Developmental Biology, Vanderbilt University Medical Center, Nashville, Tennessee 37232, USA. [3]Developmental Biology, Institute of Biology I, University of Freiburg, Hauptstrasse 1, D-79104 Freiburg, Germany. [4]Department of Surgery, Vanderbilt University Medical Center, Nashville, Tennessee 37232, USA. [5]Institute of Anatomy and Cell Biology, University of Freiburg, Albertstrasse 17, D-79104 Freiburg, Germany. [6]Nashville Veterans Administration Medical Center, Nashville, Tennessee 37212, USA. [7]Current address: Department of Biology, Box 351800, University of Washington, Seattle, Washington 98195, USA. Correspondence should be addressed to E.W.K. (ela.knapik@vanderbilt.edu).

Received 28 March; accepted 10 August; published online 17 September 2006; doi:10.1038/ng1880

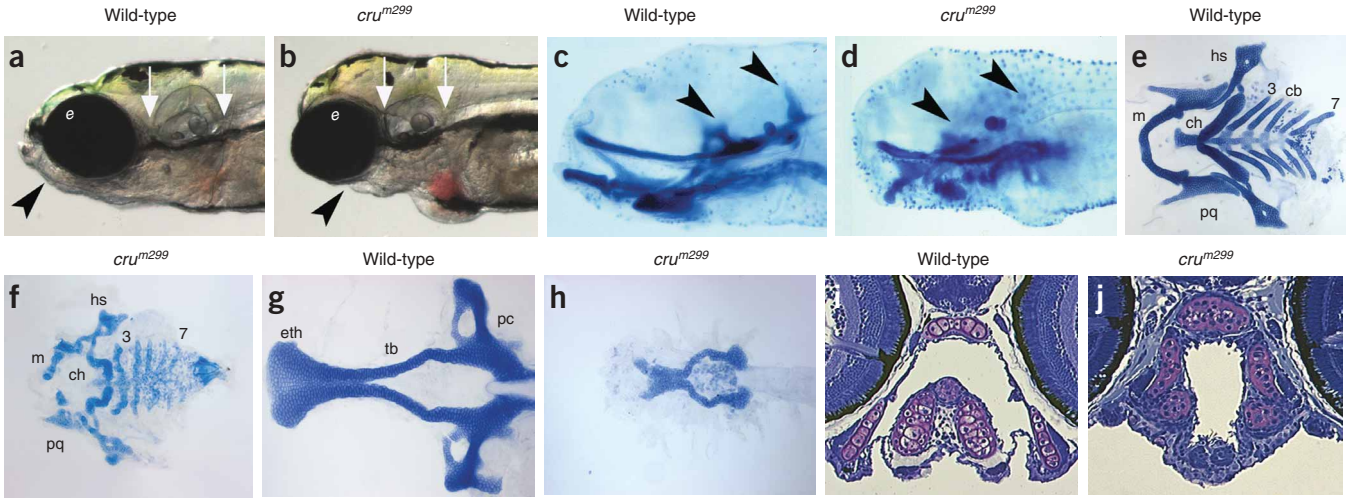

Figure 1 The *cru*^{m299} lesion disrupts craniofacial development. (**a**,**b**) Live wild-type (**a**) and *cru*^{m299} embryos (**b**) at 5 dpf. Arrowheads point to the lower jaw, and arrows demarcate the ear capsule. (**c**,**d**) Alcian blue staining of wild-type (**c**) and *cru*^{m299} (**d**) head skeletons marks cranial cartilages (arrowheads point to the ear capsule; lateral views). (**e**,**f**) Flat-mount preparation of pharyngeal skeleton shows that all cartilage elements are present in *cru*^{m299} fish (**f**), but they appear smaller and severely malformed compared with wild types (**e**). (**g**,**h**) The neurocranium of *cru*^{m299} embryos (**h**) is reduced and lacks parachordals (ear capsules). (**i**,**j**) Histological analysis, using toluidine blue staining of 5-μm transverse plastic sections of the jaw at the level of the optic nerve, shows that craniofacial chondrocytes of 5 dpf *cru*^{m299} embryos (**j**) produce ECM material (purple staining) but fail to export it to the extracellular space as in wild-type embryos (**i**). Abbreviations: e, eye; m, Meckel's cartilage; pq, palatoquadrate; ch, ceratohyal; hs, hyosymplectic; cb 3–7, ceratobranchials arches 3–7; eth, ethmoid plate; tb, trabeculae; pc, parachordals.

coding region uncovered a T→A transversion at nucleotide 1287 leading to a premature stop codon (L402X) in embryos homozygous for the *cru*^{m299} allele (**Fig. 2b**,**c**). Zebrafish Sec23a is 765 residues long, and it has been highly conserved during evolution (**Supplementary Fig. 2** online).

Because a substantial portion of the protein is not truncated by the mutation, we investigated whether knockdown of *sec23a* in wild-type embryos using translation-blocking antisense oligonucleotides would lead to more severe defects than *crusher*. However, the phenotypes of *crusher* and *sec23a* morphants were of the same severity, suggesting that the remaining domains in the truncated *sec23a* do not retain significant functional activity (**Fig. 2d**). Furthermore, knockdown of *sec23a* in embryos obtained from *crusher* heterozygote parents presented phenotypes comparable to *crusher* mutants in 95% of the injected embryos. Thus, the similar severity of the *crusher* mutant and compound *cru*^{m299}-*sec23a* morphant phenotypes suggests that the activity of Sec23a is either absent or substantially reduced in the *crusher* variant. Nevertheless, we cannot exclude the possibility that both the mutant and morphant represent hypomorphic alleles of Sec23a or that the maternally deposited *sec23a* mRNA (detected by

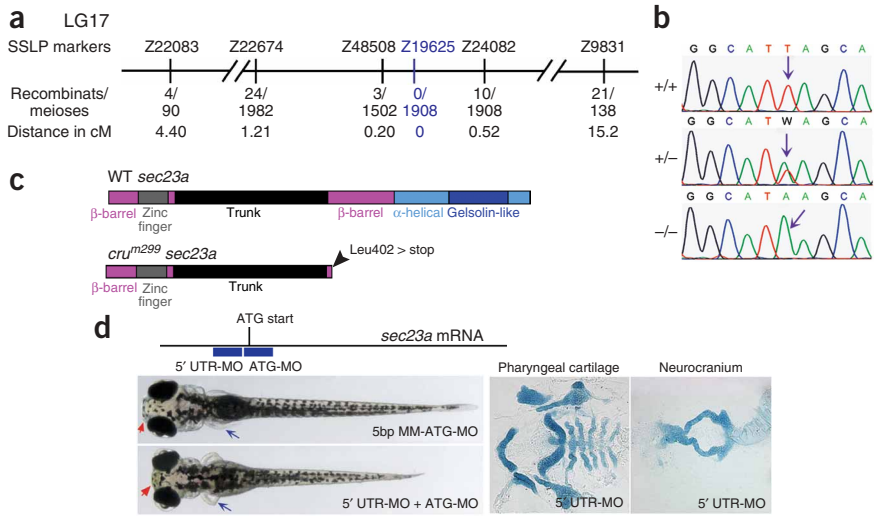

Figure 2 The *cru*^{m299} mutation is localized in the *sec23a* gene locus. (**a**) The *cru*^{m299} mutation maps to zebrafish chromosome 17 (LG 17). No recombinants were detected with the marker Z19625 in 1,908 meioses. (**b**) Electropherograms of wild-type (+/+), heterozygous (+/–) and *cru*^{m299} homozygous mutant (–/–) genomic DNA from the *sec23a* locus. The T→A transversion (arrows) results in an ochre stop codon (TAA) in place of leucine at position 402 (L402X). (**c**) Schematic diagram of the primary protein structure of Sec23a. Individual protein domains are identified in different colors. The *cru*^{m299} Sec23a mutant protein lacks part of the β-barrel domain and the entire α-helical and gelsolin-like domains. (**d**) Injection of *sec23a* antisense morpholinos (1.8 ng) results in a *cru*^{m299} phenocopy. The location of the two antisense morpholinos, in relation to the translational start site of the *sec23a* transcript, is shown above. *sec23a* morphants are morphologically indistinguishable from *cru*^{m299} mutant embryos at 4 dpf, displaying reduced body length, shorter head (red arrows) and kinked pectoral fins (blue arrows). Embryos injected with a 5-bp mismatch morpholino (5bpMM-ATG-MO) appear similar to wild-type embryos and served as controls. Flat-mounts of *sec23a* morphant pharyngeal cartilage and neurocranium stained with Alcian blue are indistinguishable from *crusher* preparations shown in **Figure 1**.

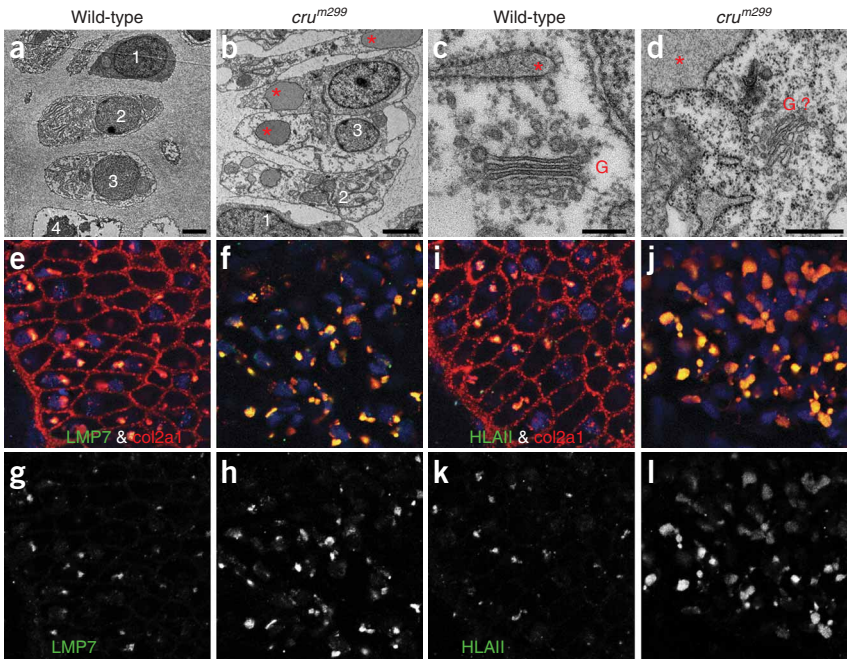

Figure 3 Transmission electron microscopy shows sparse ECM deposits and abnormal chondrocyte maturation in *cru*^{m299} embryos. (**a**,**b**) The developing wild-type cartilage (**a**) contains newly divided chondroblasts (cell 1), mature secretory chondrocytes (cell 2 and 3) and hypertrophic, non-secretory cells (cell 4). In *cru*^{m299} mutants (**b**) at 5 dpf, the cartilage matrix is considerably less dense, and large amounts of electron-dense material accumulate in the rough endoplasmic reticulum (red asterisk). (**c**,**d**) The wild-type chondrocytes (**c**) contain normal Golgi complexes and vesicles (G), whereas in *crusher* chondrocytes (**d**) the cytoplasm is filled with intracellular membranes resembling vestigial Golgi and distended endoplasmic reticulum (red asterisk). (**e**–**l**) Immunofluorescence analysis of ethmoid plate chondrocytes at 4 dpf. The antibody to collagen2α1 (red) demarcates extracellular matrix and small perinuclear areas in wild-type fish (**e**,**i**) but only juxtanuclear compartments in *crusher* (**f**,**j**). Further analysis using antibodies recognizing the proteasome LMP7 antigen (**e**–**h**) or the endoplasmic reticulum HLAII protein (**i**,**l**) (green) showed that collagen deposits in *crusher* colocalize with these compartments (yellow). The blue SYTO59 staining marks the nuclei. High-resolution single-pass, single-channel confocal images of LMP7 (**g**,**h**) and HLAII (**k**,**l**) of wild-type and *crusher* chondrocytes. Scale bars in **a** and **b** equal 2 μm; in **c** and **d**, bars represent 0.2 μm.

RT-PCR, data not shown) provides sufficient protein during early developmental stages.

Structural studies of the prebudding complex in yeast established that Sec23p interacts with Sar1p through the trunk, α-helical and gelsolin-like domains[14]. These domains are truncated in the *crusher* mutants; thus, it is conceivable that the Sec23a/Sec24 complex is unable to interact with the Sar1-GTPase to initiate cargo selection and anterograde transport. To assess whether *crusher* chondrocytes accumulate protein in the endoplasmic reticulum, upstream from the trafficking blockade, we compared electron micrographs of wild-type and *crusher* embryos (**Fig. 3a–d**). In wild-type fish, we found normal Golgi structures in maturing chondrocytes. Conversely, *crusher* chondrocytes appeared arrested in their development (**Fig. 3a**,**b**) and accumulated membranes in large and small clusters (**Fig. 3d**) that were distended and did not appear as electron dense as the wild-type Golgi complexes (**Fig. 3c**). The malformation of Golgi structures would be consistent with the cisternal maturation model, which postulates that Golgi function depends on COPII and COPI vesicle–mediated membrane recycling[8,10,11]. The *crusher* chondrocytes were distinguishable by enlarged vacuolar compartments of endoplasmic reticulum containing electron-dense material (**Fig. 3b**). In addition, the matrix deposits around chondrocytes were sparse. Accumulation of membranes and vestigial Golgi systems are consistent with the phenotype of Sec23p-deficient yeast[15], and the accumulation of large amounts of electron-dense material within the endoplasmic reticulum seems to be a characteristic feature of the *crusher* chondrocytes.

Procollagen fibrils are the primary protein product synthesized in chondrocytes, and type II collagen constitutes the majority of the cartilage extracellular matrix. To evaluate the cellular distribution of ECM proteins in *sec23a* mutants, we used an antibody recognizing collagen2α1. In wild-type cartilage, collagen2α1 was localized primarily in the extracellular space and in a small juxtanuclear compartment (**Fig. 3**). On the contrary, in *sec23a* mutants, collagen2α1 was not detectable in the extracellular space but accumulated in large vesicular structures in perinuclear areas. The intracellular deposits of collagen2α1 colocalized with the proteasome resident protein LMP7 and endoplasmic reticulum glycoprotein HLAII (**Fig. 3e–l**)[16,17]. Both proteins, LMP7 and HLAII, are expressed at higher levels in *crusher*, further suggesting increased protein handling by the proteasome and the endoplasmic reticulum (**Fig. 3g**,**h**,**k**,**l**). Moreover, glycosylation of the matrix proteins normally occurring in the Golgi complex was essentially absent in *sec23a* mutants as compared with wild-type siblings (**Fig. 4a**,**b**). These data suggest that in the Sec23a-deficient *crusher* mutants, chondrocytes accumulate large amount of ECM proteins in extended endoplasmic reticulum compartments and proteasomes, unable to transport them to the Golgi for posttranslational modifications and eventually to the extracellular matrix.

We examined how the sparsity of extracellular matrix affects the transcriptional steps of the collagen synthesis pathway[18]. Using whole-mount labeling with antisense riboprobes recognizing the mRNA of *col2a1* and transcription factor *sox9a*, which regulates collagen expression, we found that both genes are transcribed at higher levels in Sec23a mutants, especially in the pharyngeal skeleton and the ear capsule, than in wild-type siblings (**Fig. 4c**,**d**,**e**,**f**). Thus, it seems that the chondrocytes sense the absence of extracellular matrix maintaining abnormally high transcription of collagen genes. This excessive level of transcription might further exacerbate accumulation of unfolded proteins in the endoplasmic reticulum.

Abnormal accumulation in the endoplasmic reticulum of proteins, unable to continue on the secretory pathway, triggers the response of the endoplasmic reticulum quality control system, a set of folding enzymes and chaperons[19]. Indeed, expression levels of Hsp47, a chaperone responsible for folding of procollagen bundles in the endoplasmic reticulum and an integral part of the endoplasmic reticulum quality control system, are several orders of magnitude higher in *crusher* than in wild-type siblings (**Fig. 4g**,**h**).

Although Sec23p is essential in yeast[20], the zebrafish Sec23a mutants are viable up to 9 dpf. Humans and other vertebrates, including zebrafish, carry two paralogs, *SEC23A* and *SEC23B* (ref. 21). We investigated whether Sec23b might partially compensate

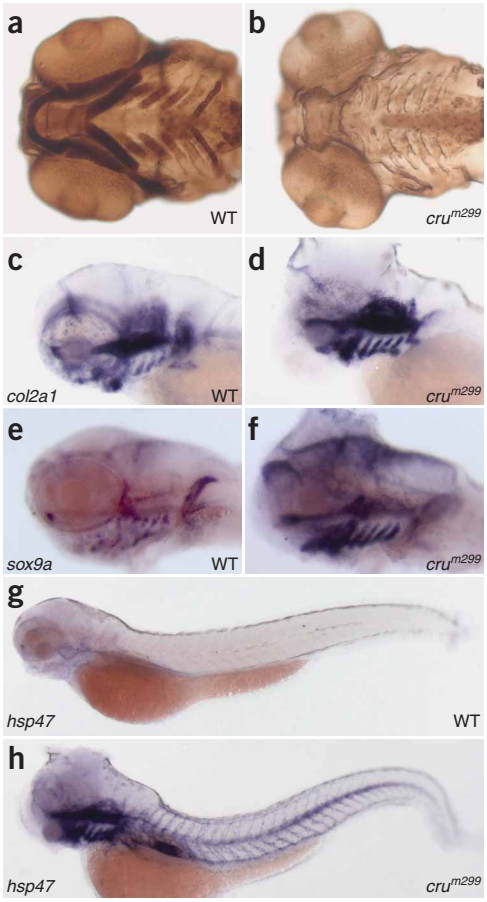

Figure 4 The Sec23a mutation disturbs glycosylation and *col2a1* expression and triggers the ER stress response. (**a**,**b**) Wheat germ agglutinin (WGA) binds to sialic acid and *N*-acetylglucosaminyl residues of proteoglycans staining glycosylated proteins. WGA binding to the ECM proteoglycans at 3 dpf is intense in the wild-type craniofacial structures (**a**), whereas in *crusher* (**b**), cartilage matrix is devoid of WGA-positive staining. (**c**,**d**) At 72 hpf, *col2a1* expression is very strong in craniofacial chondrocytes of *crusher* mutants (**d**) compared with wild-type siblings (**c**). (**e**,**f**) The expression of the *sox9a* transcription factor, which regulates *col2a1* expression, persists at high levels in craniofacial chondrocytes of cru^{m299} mutants (**f**) at 84 hpf but is downregulated in wild-type embryos (**e**). (**g**,**h**) *hsp47* transcripts in cru^{m299} mutants (**h**) at 72 hpf are maintained at high levels compared with wild-type embryos (**g**). Staining and color development of wild-type and *crusher* siblings were time matched.

for the loss of Sec23a function. To address this possibility, we blocked translation of Sec23b with a specific morpholino (**Fig. 5a**). We found that Sec23b morphants show complete loss of ventral pharyngeal skeleton, whereas neurocranium and ear capsules are similarly affected as in *crusher* (**Fig. 5**). Furthermore, the combined knockdown of Sec23a and Sec23b resulted in similar deficits in growth of the neurocranium (**Fig. 5d**,**g**,**j**). It seems that both Sec23 genes are critical in craniofacial cartilage maturation, but neither single gene activity nor the combined reduction seems essential for early zebrafish embryo survival. It is conceivable that the two genes carry specific but partially redundant roles in the secretory machinery of chondrocytes.

The collagen secretory pathway has been shown to involve the ERGIC complex, where COPI helps with cargo sorting and trafficking to the Golgi apparatus. To test the role of COPI in chondrocyte protein trafficking, we compared *crusher* to the COPI loss-of-function phenotype by injecting the previously characterized *copa* morpholino (**Fig. 6**)[22]. In COPI-deficient fish, the craniofacial skeleton was smaller but normally patterned and differentiated (**Fig. 6b**,**f**,**l**,**m**). The combined COPI and *sec23a*-deficient fish showed deficits similar to *crusher*, suggesting that *copa* does not have a role in trafficking of ECM proteins during chondrogenesis (**Fig. 6c**,**g**,**n**,**o**). Taken together, our data suggest that *sec23a* and *sec23b* are critical components of the collagen secretory pathway whereas COPI protein complexes are dispensable for ECM trafficking in chondrocytes. We further postulate that in fish, and probably in other vertebrates, there might exist additional, COPII-independent mechanisms of anterograde protein transport allowing relatively normal embryo patterning and morphogenesis. It is intriguing that although secretion is an elemental function of the cell, the most obvious phenotype appears in the craniofacial skeleton. It is possible that fast growth of the craniofacial

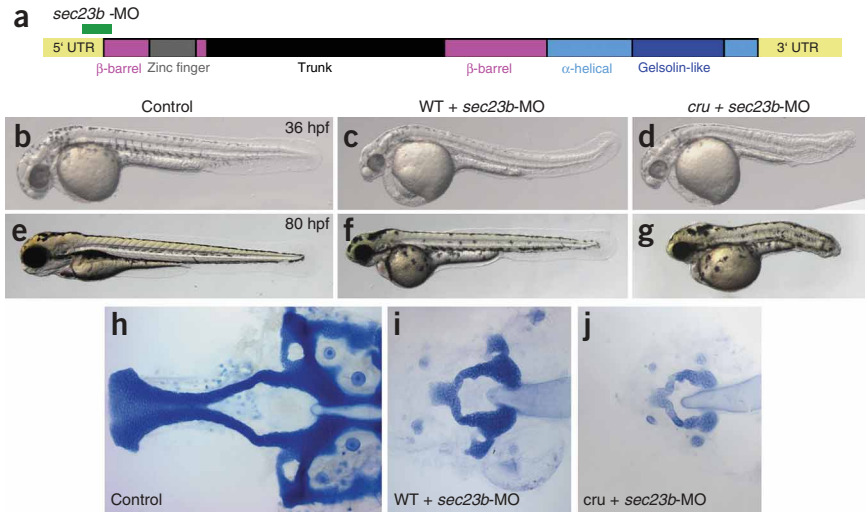

Figure 5 Knockdown of the *sec23b* gene produces a phenotype similar to cru^{m299}. (**a**) Schematic overview of the *sec23b* coding sequence and location of the *sec23b* translation-blocking antisense morpholino oligonucleotide. (**b**–**g**) Embryos obtained from cru^{m299} heterozygote crosses were injected with 3.5 ng of *sec23b* morpholino. At 36 hpf, wild-type embryos injected with *sec23b*-MO show mild growth defects and a smaller head (**c**) than uninjected controls (**b**). Injected cru^{m299} mutant embryos (**d**) show a more severe phenotype, including a shortened body axis and perturbed fin fold development. At 80 hpf, wild-type background morphants (**f**) have a slightly reduced body size and a smaller head with tissue loss in the region of the pharyngeal arches compared with uninjected controls (**e**). The severe phenotype of MO-injected cru^{m299} mutants (**g**) is characterized by short body axis, smaller head with absence of pharyngeal arches and fin fold defects. (**h**–**j**) Alcian blue-stained head cartilages (neurocranium) of 5 dpf *sec23b* morphants were dissected and flat mounted. Notably, all cartilages of the pharyngeal skeleton were missing, unlike in *sec23a* mutants (**Fig. 1f**). The loss of both *sec23* genes (**j**) results in a similar malformation but a modestly smaller neurocranium than in the case of the single loss of either Sec23b (**i**) or Sec23a (**Figs. 1h** and **2d**).

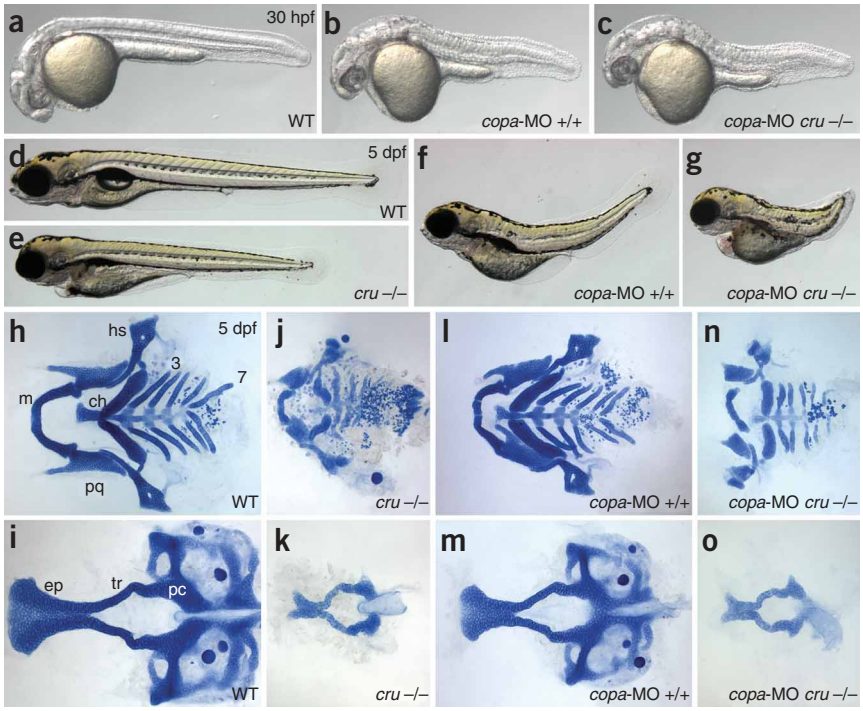

Figure 6 Knockdown of the *copa* gene does not affect chondrocyte maturation. Embryos from *cru*^{m299} heterozygote matings were injected with 0.25 ng of *copa* antisense morpholino at a concentration that phenocopied the COPI knockdown phenotype described in ref. 22. (**a**–**c**) Live fish at 30 hpf: wild-type embryos (**a**), wild-type embryos injected with *copa*-MO (**b**) and *cru*^{m299} embryos injected with *copa*-MO (**c**). The phenotypes of *copa*-MO–injected wild-type and *cru*^{m299} siblings (**b**,**c**) are almost identical at this stage. (**d**–**g**) At 104 hpf, injected wild-type embryos (**f**) are smaller than uninjected controls (**d**), have a shortened and curved body axis and fail to inflate the swim bladder but show normal head morphology compared with *crusher* (**e**). *Copa* knockdown in the *crusher* genetic background show a more severe axial skeleton phenotype that is additive to the *sec23a* defects (**g**). (**h**–**o**) Alcian blue staining of head skeletons that were dissected and flat mounted. The wild-type pattern is shown in **h** and **i**. The comparison of *crusher* pharyngeal skeleton (**j**) and neurocranium (**k**) with wild-type embryos injected with *copa*-MO (**l**,**m**) demonstrates that *copa* knockdown results in smaller but well-formed neurocranium and cartilage that closely resemble the wild-type pattern (**h**,**i**) in shape and staining intensity. Unlike the trunk and tail phenotype, the pharyngeal skeleton defects after *copa*-MO injection in *cru*^{m299} (**n**,**o**) are practically identical to the phenotype of uninjected *cru*^{m299} embryos (**j**,**k**), suggesting that the loss of COPI does not further exacerbate the deficit of COPII function in craniofacial cartilage. Abbreviations for cartilage elements as in **Figure 1**.

skeleton makes chondrocytes hypersensitive to the trafficking speed of the secretory pathway. This would be consistent with the *crusher* phenotype that becomes first visible when the chondrocytes start ramping up protein production and cartilages begin rapid isometric growth. Other cell types might not be as sensitive to the cargo transport efficiency, either because a small portion of COPII is still operational or because cells use alternative shipment strategies.

An increasing number of human disorders are being attributed to mutations in the genes of the intracellular protein trafficking machinery, but the pathophysiology of these diseases is poorly understood. For example, lesions in the COPII complex component SARA2 have been identified as the etiology of the chylomicron retention disease, Anderson disease and Marinesco-Sjogren syndrome, resulting in lipid malabsorption in infants and failure to thrive[23]. Recently, the craniolenticulo-sutural dysplasia (CLSD) syndrome has been mapped to human chromosome 14q13-q21 (ref. 24). The syndrome is characterized by mild generalized skeletal dysplasia, open cranial sutures, hypertelorism, frontal bossing, broad prominent nose and cataracts. The human chromosome 14q13 is syntenic to zebrafish chromosome 17, where the *crusher*^{m299} mutation maps. In this issue[25], another group shows that a private SNP variant in human *SEC23A* is responsible for the CLSD disorder. Thus, the *crusher* mutation corresponds to the genetic etiology of the human disease CLSD, representing the first vertebrate model system that links the biology of endoplasmic reticulum–to–Golgi trafficking with a clinically relevant dysmorphology.

METHODS

Zebrafish maintenance and breeding. Fish were raised and maintained as previously described[26,27]. The *cru*^{m299} allele[12] was kept in the AB genetic background for phenotypic analysis and crossed to the WIK line for genetic mapping[13]. All zebrafish experiments were approved by the Institutional Animal Care and Use Committee at the Vanderbilt University.

Cartilage proteoglycan staining. Alcian blue staining was done as previously described[12,27]. Embryos at 5 dpf were fixed in 4% phosphate-buffered paraformaldehyde (PFA), bleached in 10% hydrogen peroxide (H_2O_2) and 2 M KOH and stained overnight in 0.1% Alcian blue solution.

Histology. We fixed 5 dpf wild-type and homozygous *crusher*^{m299} embryos in 4% PFA, dehydrated them to 95% ethanol, embedded them in JB-4 resin (Polysciences), sectioned them at 5 μm thickness using a Reichert OmU3 microtome and stained with the metachromatic dye toluidine blue.

Wheat germ agglutinin staining for glycosylated proteins. Embryos were fixed and labeled with biotinylated wheat germ agglutinin (Vector Laboratories, 5 mg/ml) at 1:2,800 dilution. The color reaction was developed using the Vectastain ABC kit with horseradish peroxidase and diaminobenzidine as chromogen (Vector Laboratories).

Genetic mapping and cloning. The *cru*^{m299} locus was mapped in a F2 intercross using bulked segregant analysis. DNA samples were genotyped by PCR with SSLP (simple sequence length polymorphism) markers evenly spaced across the zebrafish genome[13]. Using 1,950 meioses, we mapped the *cru*^{m299} mutation to an interval of 0.72 cM between markers Z48508 and Z24082, with no recombinants to Z19625. Comparison of zebrafish and human syntenic regions identified EST fi15g03, encoding *sec23a*, as a potential candidate gene. Zebrafish *sec23a* cDNA is 5,556 bp long, and the ORF of 2,298 bp encodes a protein of 765 amino acids. The *cru*^{m299} mutation in putative exon 10 (1287T→A transversion) has been confirmed by sequencing of three homozygous wild-type F2 animals, six *cru*^{m299} heterozygous F2 animals, six homozygous *cru*^{m299} mutant F2 animals and seven adult F1 heterozygotes with primers sec23a-seq1F and sec23a-seq1R (**Supplementary Table 1** online). In addition, two random animals each of the wild-type lines AB, HK, IN, TL and WIK tested negative for the mutation.

Antibodies and immunofluorescence. Immunofluorescence experiments were done essentially as described[27] with 1:100 diluted primary antibodies against collagen type II (Polysciences), HLAII (LGII-612.14) and LMP7 (both gifts of S. Ferrone). Alexa Fluor 488 and Alexa Fluor 555 (Molecular Probes) were

applied as fluorescently conjugated secondary antibodies (1:400). Nucleic acid stain SYTO59 (Molecular Probes; 1:10,000) was used to label cell nuclei. Confocal images were taken with a Zeiss LSM510 Meta in the Vanderbilt Cell Imaging Shared Resource.

***In situ* hybridization.** Whole-mount *in situ* hybridization was performed as described[27]. The following probes were used: *col2a1* (ref. 28), *hsp47* (ref. 29) and *sox9a* (ref. 30). All pair-wise stainings are time matched, but the reactions were stopped when the *crusher* embryos reached maximum staining and we could still distinguish individual cartilage elements. Specifically, *hsp47* staining was stopped after several minutes, which is too short a time for the wild-type pattern to appear.

Morpholino knockdown. Antisense morpholino (MO) oligonucleotides (Gene Tools) were targeted to the *sec23a* 5′ untranslated region (*sec23a*-MO$^{5'UTR}$); the *sec23a* 5′ translation start site (*sec23a*-MO^{AUG}) and the *sec23b* translation start site (*sec23b*-MO). Morpholino sequences are listed in **Supplementary Table 1**. The *copa* morpholino was used as previously described[22]. Control mismatch morpholinos were provided by Gene Tools. Morpholino concentrations were determined spectrophotometrically, and 1 nl was injected into one- to four-cell-stage embryos at increasing doses (0.5 ng–10 ng) to determine optimal concentrations. Working doses for each morpholino are listed in the figure legends.

Transmission electron microscopy (TEM). For TEM, day 5 embryos were fixed in 2.0% glutaraldehyde and 1.0% paraformaldehyde in PBS. Specimens were postfixed with 1.0% osmium tetroxide and stained with 1.0% uranyl acetate.

Accession codes. GenBank: zebrafish *sec23a* cDNA, BC052768; zebrafish *sec23b* cDNA, BC045394.

Note: Supplementary information is available on the Nature Genetics website.

ACKNOWLEDGMENTS

We thank C. Knappmeyer and S. Goetter for excellent zebrafish animal care; B. Joch for electron microscopy; S. Ferrone for LMP7 and HLAII antibodies; W. Driever for sharing the *crusher* mutant and wild-type zebrafish lines and L. Beihoffer for performing supporting experiments. We are indebted to A. Hatzopoulos, T. Graham, A. George and M. Summers for critically reading the manuscript and S. Wente for discussions. This work has been supported in part by the zebrafish initiative of the Vanderbilt University Academic Venture Capital Fund (E.W.K.).

AUTHOR CONTRIBUTIONS

M.R.L. conducted all experiments except electron microscopy by M.F. and confocal imaging by L.A.L. The project was designed and orchestrated by E.W.K., who analyzed the data and wrote the paper. All authors discussed the results and commented on the manuscript.

COMPETING INTERESTS STATEMENT

The authors declare that they have no competing financial interests.

Published online at http://www.nature.com/naturegenetics
Reprints and permissions information is available online at http://npg.nature.com/reprintsandpermissions/

1. Bonifacino, J.S. & Glick, B.S. The mechanisms of vesicle budding and fusion. *Cell* **116**, 153–166 (2004).
2. Yoshihisa, T., Barlowe, C. & Schekman, R. Requirement for a GTPase-activating protein in vesicle budding from the endoplasmic reticulum. *Science* **259**, 1466–1468 (1993).
3. Hicke, L. & Schekman, R. Yeast Sec23p acts in the cytoplasm to promote protein transport from the endoplasmic reticulum to the Golgi complex in vivo and in vitro. *EMBO J.* **8**, 1677–1684 (1989).
4. Mellman, I. & Warren, G. The road taken: past and future foundations of membrane traffic. *Cell* **100**, 99–112 (2000).
5. Stagg, S.M. *et al.* Structure of the Sec13/31 COPII coat cage. *Nature* **439**, 234–238 (2006).
6. Matsuoka, K. *et al.* COPII-coated vesicle formation reconstituted with purified coat proteins and chemically defined liposomes. *Cell* **93**, 263–275 (1998).
7. Mironov, A.A. *et al.* ER-to-Golgi carriers arise through direct en bloc protrusion and multistage maturation of specialized ER exit domains. *Dev. Cell* **5**, 583–594 (2003).
8. Bonfanti, L. *et al.* Procollagen traverses the Golgi stack without leaving the lumen of cisternae: evidence for cisternal maturation. *Cell* **95**, 993–1003 (1998).
9. Stephens, D.J. & Pepperkok, R. Imaging of procollagen transport reveals COPI-dependent cargo sorting during ER-to-Golgi transport in mammalian cells. *J. Cell Sci.* **115**, 1149–1160 (2002).
10. Presley, J.F. *et al.* ER-to-Golgi transport visualized in living cells. *Nature* **389**, 81–85 (1997).
11. Scales, S.J., Pepperkok, R. & Kreis, T.E. Visualization of ER-to-Golgi transport in living cells reveals a sequential mode of action for COPII and COPI. *Cell* **90**, 1137–1148 (1997).
12. Neuhauss, S.C. *et al.* Mutations affecting craniofacial development in zebrafish. *Development* **123**, 357–367 (1996).
13. Knapik, E.W. *et al.* A microsatellite genetic linkage map for zebrafish (Danio rerio). *Nat. Genet.* **18**, 338–343 (1998).
14. Bi, X., Corpina, R.A. & Goldberg, J. Structure of the Sec23/24-Sar1 pre-budding complex of the COPII vesicle coat. *Nature* **419**, 271–277 (2002).
15. Novick, P., Field, C. & Schekman, R. Identification of 23 complementation groups required for post-translational events in the yeast secretory pathway. *Cell* **21**, 205–215 (1980).
16. Bandoh, N. *et al.* Development and characterization of human constitutive proteasome and immunoproteasome subunit-specific monoclonal antibodies. *Tissue Antigens* **66**, 185–194 (2005).
17. Gebe, J.A., Swanson, E. & Kwok, W.W. HLA class II peptide-binding and autoimmunity. *Tissue Antigens* **59**, 78–87 (2002).
18. Bell, D.M. *et al.* SOX9 directly regulates the type-II collagen gene. *Nat. Genet.* **16**, 174–178 (1997).
19. Ma, Y. & Hendershot, L.M. ER chaperone functions during normal and stress conditions. *J. Chem. Neuroanat.* **28**, 51–65 (2004).
20. Kaiser, C.A. & Schekman, R. Distinct sets of SEC genes govern transport vesicle formation and fusion early in the secretory pathway. *Cell* **61**, 723–733 (1990).
21. Paccaud, J.P. *et al.* Cloning and functional characterization of mammalian homologues of the COPII component Sec23. *Mol. Biol. Cell* **7**, 1535–1546 (1996).
22. Coutinho, P. *et al.* Differential requirements for COPI transport during vertebrate early development. *Dev. Cell* **7**, 547–558 (2004).
23. Jones, B. *et al.* Mutations in Sar1 GTPase of COPII vesicles are associated with lipid absorption disorders. *Nat. Genet.* **34**, 29–31 (2003).
24. Boyadjiev, S.A. *et al.* A novel dysmorphic syndrome with open calvarial sutures and sutural cataracts maps to chromosome 14q13-q21. *Hum. Genet.* **113**, 1–9 (2003).
25. Boyadjiev, S.A. *et al.* Cranio-lenticulo-sutural dysplasia is caused by a *SEC23A* mutation leading to abnormal ER-to-Golgi trafficking. *Nat. Genet.* published online 17 September 2006 (doi:10.1038/ng1876).
26. Kimmel, C.B., Ballard, W.W., Kimmel, S.R., Ullmann, B. & Schilling, T.F. Stages of embryonic development of the zebrafish. *Dev. Dyn.* **203**, 253–310 (1995).
27. Barrallo-Gimeno, A., Holzschuh, J., Driever, W. & Knapik, E.W. Neural crest survival and differentiation in zebrafish depends on mont blanc/tfap2a gene function. *Development* **131**, 1463–1477 (2004).
28. Yan, Y.L., Hatta, K., Riggleman, B. & Postlethwait, J.H. Expression of a type II collagen gene in the zebrafish embryonic axis. *Dev. Dyn.* **203**, 363–376 (1995).
29. Pearson, D.S., Kulyk, W.M., Kelly, G.M. & Krone, P.H. Cloning and characterization of a cDNA encoding the collagen-binding stress protein hsp47 in zebrafish. *DNA Cell Biol.* **15**, 263–272 (1996).
30. Chiang, E.F. *et al.* Two sox9 genes on duplicated zebrafish chromosomes: expression of similar transcription activators in distinct sites. *Dev. Biol.* **231**, 149–163 (2001).